Journal of Catalysis 285 (2012) 41–47

Contents lists available at SciVerse ScienceDirect

Journal of Catalysis

journal homepage: www.elsevier.com/locate/jcat

Influence of bulk composition of the intermetallic compound ZnPd on surface composition and methanol steam reforming properties

Matthias Friedrich [a], Detre Teschner [b], Axel Knop-Gericke [b], Marc Armbrüster [a,*]

[a] Max-Planck-Institut für Chemische Physik fester Stoffe, Nöthnitzer Straße 40, 01187 Dresden, Germany
[b] Inorganic Chemistry Department, Fritz-Haber-Institute of the Max-Planck-Society, Faradayweg 4-6, 14195 Berlin, Germany

ARTICLE INFO

Article history:
Received 10 June 2011
Revised 22 August 2011
Accepted 12 September 2011
Available online 14 October 2011

Keywords:
Methanol steam reforming
Heterogeneous catalysis
ZnPd
PdZn
Intermetallic compound
XPS
In situ

ABSTRACT

Single-phase samples of the intermetallic compound ZnPd, all possessing the CuAu type of crystal structure, were prepared with different bulk compositions and characterized by ICP-OES and XRD. Catalytic experiments in methanol steam reforming in a flow reactor on the unsupported intermetallic compounds proved that Pd-rich catalysts showed limited activity and very low selectivity to CO_2, while Zn-rich catalysts possessed good activity and CO_2 selectivity up to 99.4%. XP spectra of the near-surface region were recorded on as-prepared and reduced samples, showing significant variations in Zn/Pd surface ratios, Pd3d binding energies and the amount of oxidized Zn species on the surface. These properties were correlated with the Pd content of the bulk compounds. *In situ* XPS studies revealed that only Zn-rich samples exhibited oxidized Zn species and intermetallic ZnPd on the surface. The catalytic properties correlate strongly with the electronic structure, i.e., the valence band which is determined by the bulk composition. All ZnPd samples still revealed a partially intermetallic near-surface region under MSR conditions.

1. Introduction

Methanol steam reforming (MSR, $CH_3OH + H_2O \rightarrow 3H_2 + CO_2$) is paid high attention because it is considered as one of the most promising routes to produce high purity hydrogen for fuel cell applications [1]. The main drawback, still hindering application, is the formation of CO as byproduct. Above a level of 10 ppm, it poisons fuel cell catalysts converting hydrogen to electricity [2]. Conventional catalysts for methanol steam reforming are Cu/ZnO/Al_2O_3 and other Cu-based systems, producing at least 1100 ppm of CO [3,4]. Limited long-term stability due to sintering at elevated temperatures and the pyrophoric nature of these catalysts are further drawbacks. Noble-metal-based systems were introduced to circumvent some of the problems. Pd supported on hard-to-reduce oxides M_xO_y (M = Si, Al, Mg) solely catalyzes the decomposition of methanol to CO and H_2. Using oxides like ZnO, Ga_2O_3 or In_2O_3 as support for Pd changes the selectivity toward CO_2 [5–7]. The formation of intermetallic compounds like ZnPd, Ga_5Pd, Ga_2Pd_5 and InPd by reactive metal-support interactions (RMSI) is observed on these catalysts after the catalytic reaction [8]. These intermetallic compounds are held responsible for the increased CO_2 selectivity of the supported catalysts. The initial Pd/ZnO catalyst, forming the intermetallic compound ZnPd on the surface upon reduction and even under methanol steam reforming conditions [9], is the most interesting system, because a CO_2 selectivity of 99.5% was reported [8]. To date, the role of the intermetallic compound ZnPd, the ZnO support and the corresponding interface is intensively discussed [10,11]. Does the high CO_2 selectivity solely originate from the intermetallic compound, even if no ZnO, either as support or as impurity, is present? ZnPd/C was shown to maintain the high CO_2 selectivity of ZnPd/ZnO, but even the reduced catalyst still possessed large amounts of ZnO on the surface, hindering a proper assignment of catalytic properties to the respective compounds [12]. Tsai et al. investigated a series of unsupported intermetallic compounds, including ZnPd, in methanol steam reforming and concluded that the electronic structure of the intermetallic compounds in particular the density of states at the Fermi edge may directly be related to the catalytic selectivity of these intermetallic compounds in MSR [13]. Follow-up work of the same group reported on the synthesis of unsupported, single-phase ZnPd, obtained by leaching of the intermetallic compound $Al_{21}Pd_8$ with aqueous $ZnCl_2$ solution and reduction in hydrogen [14]. In these studies, the *in situ* stability of the intermetallic compounds was not investigated and the presence of oxidized surfaces was not considered. Another unconventional approach to synthesize the intermetallic compound ZnPd in the unsupported state was realized using an aerosol-derived method that yielded micro-sized homogeneous intermetallic particles, but the oxidation of some Zn on the surface could not be avoided [15,16]. The investigation into ZnPd near-surface alloys showed a significant influence of the composition of the ZnPd surface layers on the catalytic

* Corresponding author.
E-mail address: marc.armbruester@cpfs.mpg.de (M. Armbrüster).

0021-9517/$ - see front matter © 2011 Elsevier Inc. All rights reserved.
doi:10.1016/j.jcat.2011.09.013

selectivity in MSR [17,18]. Hence, reviewing the existing literature on ZnPd or related catalytic systems leads to the conclusion that unsupported, oxide-free intermetallic surfaces are necessary to clarify the role of the intermetallic compound ZnPd in methanol steam reforming. Using unsupported intermetallic compounds reduces the complexity of the catalytic system and is beneficial for knowledge-based studies in catalysis [19,20].

In this work, single-phase samples of the intermetallic compound $Zn_{100-x}Pd_x$ (x = 46.8–59.1) were prepared as unsupported metallic powders with different compositions within the homogeneity range. After bulk characterization by XRD and ICP-OES, the $Zn_{100-x}Pd_x$ samples were tested as unsupported catalysts in methanol steam reforming in a flow reactor. To correlate the catalytic results at atmospheric pressures with the state of the surface, XPS using synchrotron radiation in UHV and under methanol steam reforming conditions at 0.2 mbar was applied to detect changes of the surface after different pretreatments as well as under *in situ* conditions.

2. Methods

$Zn_{100-x}Pd_x$ samples were synthesized by heating elemental Zn and Pd in the respective atomic ratio in an evacuated and sealed quartz glass ampoule until 900 °C and annealing for 6 days [21]. All steps of the synthesis were carried out in a glove-box (Ar atmosphere, O_2 and H_2O levels below 0.1 ppm). No interaction of the reaction educts with the quartz glass was observed. Phase purity of the samples was verified by X-ray powder diffraction (Huber image plate G670, Cu Kα_1, a = 1.54056 Å, quartz monochromator, $3° < 2\theta < 100°$). The unit cell parameters were determined using the program WinCSD [22] and LaB_6 as internal standard (a = 4.15692 Å). To determine chemical compositions, the intermetallic samples were dissolved in aqua regia and subsequently analyzed in triplicate by ICP-OES (Vista RL, Varian) after matrix-matched calibration. In general, samples analyzed by ICP-OES showed to be lean in Pd by up to 1 at% compared to the initially weighted Pd and Zn amounts. This might be due to the use of fine Pd powder that is prone to stick to quartz glass surfaces during sample preparation. Standard deviations of the ICP-OES analyses are given in Fig. 1 (inset).

Catalytic measurements were taken in a flow reactor system (Microactivity Reference, PID Eng&Tech). Prior to the catalytic tests, the $Zn_{100-x}Pd_x$ samples were ground in air, sieved to a size smaller than 20 μm and mixed with 200 mg of graphite (Chempur, 99.9+%), which is catalytically inactive in MSR, to dilute the catalyst bed. Sample amounts were in the range of 100–150 mg. The catalyst was placed inside a silica-coated stainless steel tube (inner diameter 7.9 mm) which was mounted inside a heated box to prevent condensation of liquids. The reactive feed consisted of 0.01 mL/min liquid (50 mol.-% MeOH (purity >99%), 50 mol.-% deionized water) which is evaporated before being mixed with 13.2 mL/min N_2 and 1.6 mL/min He (both Praxair, 99.999%). N_2 was used as carrier gas, while He was applied as inert tracer gas to calibrate the gas volumes. The gas composition in the product stream was determined by a gas chromatograph (Varian Micro GC CP4900), allowing quantitative and qualitative determination of CO of 20 and 5 ppm, respectively. Amounts of unconverted MeOH and H_2O as well as the potential product formaldehyde were not determined by GC because they were separated from the product gas by a cooling trap and a subsequent Nafion® membrane before being injected into the GC. The conversion of MeOH and H_2O was calculated as $C = (H_{2\_out}/H_{2\_max}) \times 100$, wherein H_{2_out} is the amount of H_2 in the product gas and H_{2_max} is the amount of H_2 that can be generated if all MeOH and H_2O are converted according to the reaction equation $CH_3OH + H_2O \rightarrow 3H_2 + CO_2$. The product fractions were calculated by dividing the concentration of one product by the sum of the concentration of all products, disregarding the inert gases N_2 and He. To identify all gaseous compounds, including formaldehyde, a mass spectrometer (Pfeiffer Omnistar) was connected to the gas outlet before the separation procedure. For the Pd-rich samples, the produced H_2 occasionally accounted for more than 80% in the $H_2/CO_2/CO$ mixture as analyzed by the GC. Since methanol steam reforming and methanol decomposition can only yield a maximum of 75% and 66% H_2, respectively, another carbon containing product must have been formed which was identified as formaldehyde by mass spectrometry.

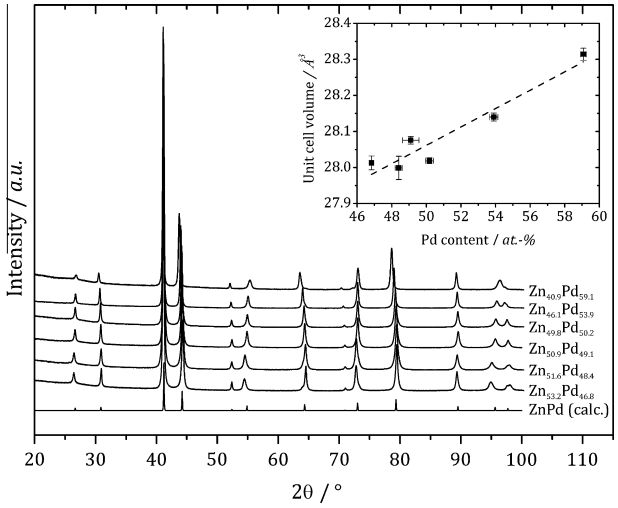

Fig. 1. X-ray powder diffraction of as-prepared $Zn_{100-x}Pd_x$ samples with different compositions in comparison with the calculated XRD pattern for tetragonal ZnPd ($P4/mmm$, CuAu type of structure, a = 2.8931 Å, c = 3.3426 Å). The inset shows the Pd-bulk content from ICP-OES analysis vs. unit cell volume as derived from XRD.

XPS measurements in the mbar regime using synchrotron radiation were taken at beamline ISISS-PGM at the Helmholtz Zentrum Berlin für Materialien und Energie – Electron storage ring BESSY II. A detailed description of the setup can be found elsewhere [23]. 150–200 mg of each ZnPd sample were ground and pressed in air to pills of 8 mm in diameter and 0.5–1 mm in thickness using stainless steel pressing tools. Investigation into the surface of the as-prepared samples was carried out at room temperature and at pressures of 10^{-8} mbar. Reduction in hydrogen was performed *in situ* at 0.5 mbar H_2 pressure and at different temperatures while recording the Zn Auger LMM region to detect remaining oxidized Zn species on the surface. *In situ* experiments were carried out at 0.2 mbar and at different temperatures using a H_2O/MeOH ratio of 2:1. Since only low catalytic conversion could be realized within the XPS cell, the formation of hydrogen – monitored by a mass spectrometer (Pfeiffer Prisma) – was taken as a qualitative indicator of catalytic activity. Other reaction products like CO, CO_2 or formaldehyde were monitored as well. Depth profiles of the samples were collected in every state of the sample (as-prepared, after reduction, *in situ* MSR) by using up to nine different photon energies for the measurement of the respective core levels (Pd3d, Zn3d, O1s, C1s). For each spectrum, the Fermi edge at the corresponding photon energy was measured for energy calibration. The software Casa XPS [24] was used for qualitative and quantitative analyses of the XP spectra. To calculate Zn/Pd and metal/carbon ratios, the respective peak areas were corrected considering ring current, photon flux and tabulated cross sections [25].

3. Results and discussion

3.1. Characterization of as-prepared samples

A recent investigation into the chemical bonding and phase region of the intermetallic compound ZnPd (tetragonal, space

group *P*4/*mmm*, CuAu type of crystal structure) confirmed the broad homogeneity range of 46–63 at% Pd [21]. Combining experimental and theoretical aspects led to the conclusion that the cubic high-temperature modification of ZnPd does not exist. XRD confirmed that all samples used in this study were single-phase and only contained tetragonal CuAu-type ZnPd. Fig. 1 shows X-ray powder diffraction patterns of samples with different composition in comparison with the calculated pattern for tetragonal ZnPd (50 at% Pd, ideal structural model). With increasing Pd content, the lattice parameters *a* and *c* are increasing and decreasing, respectively (Fig. S1). The compositional dependency of the unit cell volume (Fig. 1, inset) reveals a Vegard-like behavior.

The $Zn_{100-x}Pd_x$ (x = 46.8–59.1) samples were investigated by XPS to explore the near-surface region of the intermetallic compounds. Fig. 2 shows depth profiles of the Zn3d and the $Pd3d_{5/2}$ regions of $Zn_{51.6}Pd_{48.4}$, which are representative for all investigated $Zn_{100-x}Pd_x$ samples in the as-prepared state. For the Zn3d region at the most surface-sensitive photon energy (237 eV), two different Zn species could be identified, both of which were fitted according to their spin orbit splitting. The peak at a binding energy (BE) of 10.6 eV is assigned to oxidized Zn, whereas the peak at 9.25 eV is ascribed to Zn in the intermetallic compound ZnPd. Both assignments are in line with the fact that the relative signal intensity of the oxidized Zn species at 10.6 eV decreases toward the bulk, which is the intermetallic compound $Zn_{100-x}Pd_x$, while the relative signal intensity of the intermetallic Zn species at 9.25 eV increases. The oxidized Zn species is assumed to originate from the presence of zinc oxide and does not shift with increasing photon energies. Fitting parameters for the Zn3d signals are given in Table S1. Depth profiling of the $Pd3d_{5/2}$ region of $Zn_{51.6}Pd_{48.4}$ shows an obvious shift of the $3d_{5/2}$ signal with increasing photon energy (Fig. 2b). Elemental Pd can be excluded because the BE of the observed signal is significantly above its typical value of 335 eV [26]. If oxidized Pd would be present, i.e., due to the interaction of Pd atoms and oxygen on the surface, a signal should be observed at 336.55 eV [27], which is not the case. Furthermore, the continuous shift of the Pd3d signal to higher BE with increasing photon energy is another indication for not being of oxidic nature. The good resolution of the spectra allows detecting asymmetries in the peak shape revealing that more than one species is necessary to fit the $Pd3d_{5/2}$ signal, resulting from the fluent change in composition from the surface to the bulk composition as determined by ICP-OES (Fig. 2c). Because of the different crystal structures of elemental Pd (fcc) and ZnPd (tetragonal CuAu type of crystal structure), the shift in BE from Pd (335 eV) to ZnPd (336 eV) is not realized by adding Zn to the Pd lattice as in the case of alloys according to the rigid band theory. Therefore, it is necessary to qualitatively and quantitatively analyze the spectra (Fig. 2b and c). The changing composition leads to small changes of the local electronic concentration in the intermetallic compound with increasing depth, resulting in slightly different BEs.

The surface after preparation is characterized by Zn enrichment which is mostly present as zinc oxide. This effect is caused by the sample preparation. The powders of the intermetallic $Zn_{100-x}Pd_x$ samples were ground and pressed in air prior to the XPS measurements. Grinding causes mechanical and thus energetic impact on the surface leading segregation of the Zn atoms and their oxidation due to the presence of oxygen, an observation that has also been made on the isostructural intermetallic compound ZnPt after milling [28]. If Zn segregation takes place, the electronic structure changes according to the Pd content, leading to depth-depending BE shifts.

3.2. Surface analysis of reduced $Zn_{100-x}Pd_x$ samples

All $Zn_{100-x}Pd_x$ samples underwent a reductive treatment at elevated temperatures in the XPS chamber to restore the intermetallic

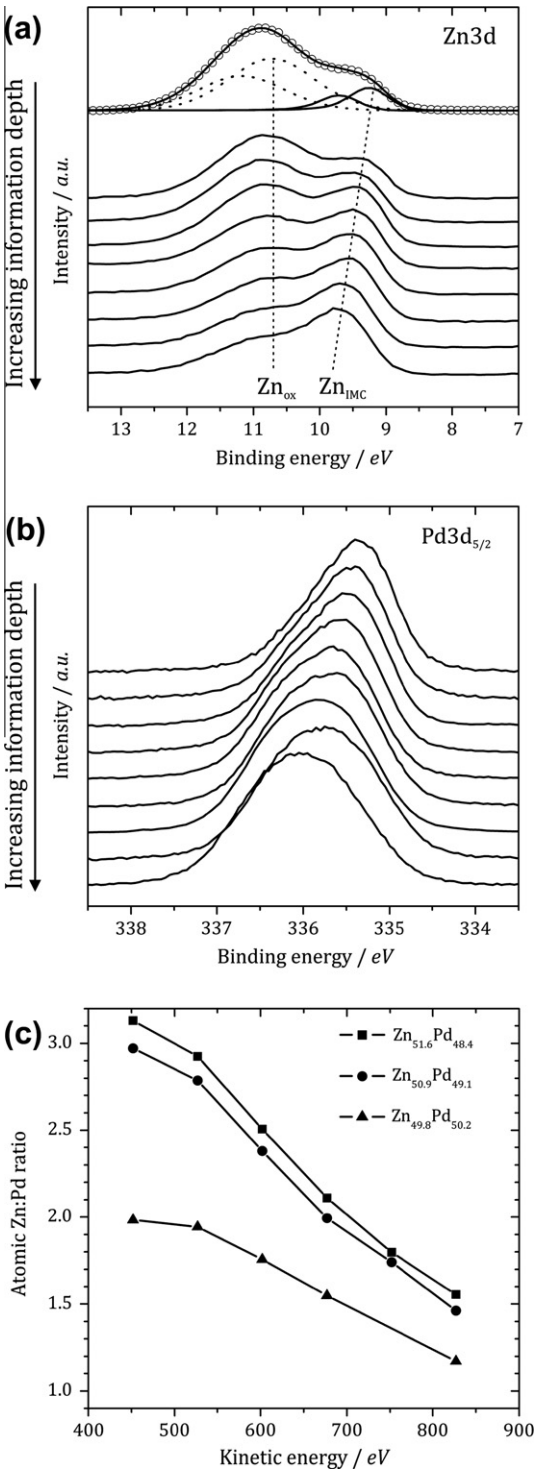

Fig. 2. (a and b) XPS of as-prepared $Zn_{51.6}Pd_{48.4}$. Top spectra correspond to photon energies of 237 eV (a) and 562 eV (b), respectively. Photon energies have been increased in steps of 75 eV to record the other spectra. Depth-depending atomic Zn/Pd ratio of as-prepared $Zn_{51.6}Pd_{48.4}$, $Zn_{50.9}Pd_{49.1}$ and $Zn_{49.8}Pd_{50.2}$ (c).

character of the surface to its possible extent. During the whole reductive treatment, spectra of the Zn Auger LMM region were recorded to discriminate between metallic and oxidized Zn species. First, the samples were exposed to 0.5 mbar H_2 pressure at room temperature. The reduction temperature was then raised to 240 °C with 12 K/min, held for 10 min and further increased stepwise by 60 °C with 24 K/min. Heating was continued until 420 °C for each sample and kept at this temperature until the Zn Auger

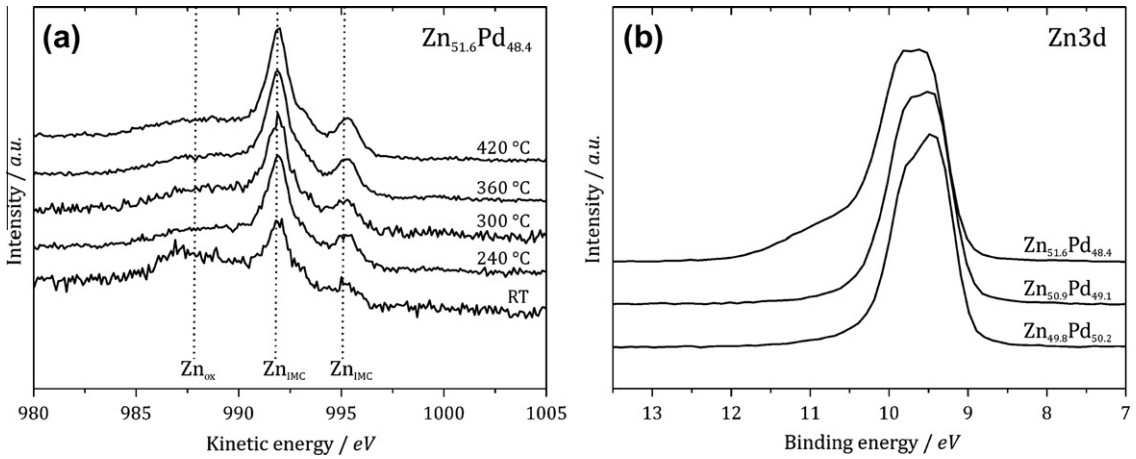

Fig. 3. (a) Zn LMM Auger signals of $Zn_{51.6}Pd_{48.4}$ during *in situ* reduction in H_2 (0.5 mbar) at different temperatures (photon energy = 1400 eV). (b) XPS Zn3d region of $Zn_{100-x}Pd_x$ samples after *in situ* reduction in H_2 (420 °C, 0.5 mbar, photon energy = 237 eV).

LMM signals showed no changes. Fig. 3a shows reduction in the intensity of the oxidic Zn signal in $Zn_{51.6}Pd_{48.4}$ (representative for all ZnPd samples), while the signal for intermetallic Zn strongly increased. To get a detailed picture of the surface states after the reduction procedure, complete depth profiles (Pd3d, Zn3d, O1s, C1s) were recorded in UHV at room temperature again for all samples. Fig. 3b shows the Zn3d region of three samples ($Zn_{51.6}Pd_{48.4}$, $Zn_{50.9}Pd_{49.1}$ and $Zn_{49.8}Pd_{50.2}$) for the most surface-sensitive photon energy (237 eV) after reduction in H_2 at 420 °C. For $Zn_{51.6}Pd_{48.4}$, the shoulder at higher BE in the Zn3d spectra is assigned to oxidized Zn that could not be reduced under these conditions, while the Pd-rich samples showed only one doublet signal with an asymmetric tail at higher BE. Depth profiling of the Zn3d region for the Pd-rich samples (not shown) revealed no changes in the asymmetric peak shape, indicating that oxidized Zn cannot be present in these spectra. This is further supported by the lack of the O1s signal of the Pd-rich samples (Fig. S2). In this spectral region, O1s – typically at 530 eV [27] – and $Pd3p_{3/2}$ overlap, and an estimation of the expected O1s and $Pd3p_{3/2}$ intensities led to the conclusion that the Pd-rich $Zn_{100-x}Pd_x$ samples are likely to be free of oxygen. In contrast, 13 at% of the total amount of Zn of the Zn-rich sample $Zn_{51.6}Pd_{48.4}$ at the photon energy of 237 eV remained oxidized after the reductive treatment.

The $Pd3d_{5/2}$ spectra of the depth profiles of the three selected $Zn_{100-x}Pd_x$ samples after reduction in hydrogen at 420 °C are shown in Fig. 4. The depth profiles show significant differences depending on the bulk composition of the samples. All three depth profiles have in common that the $Pd3d_{5/2}$ signals shift to higher BE with increasing photon energy. This shift was already observed for the as-prepared samples (Fig. 2b) and was assigned to the change of the local electronic structure due to the increasing Pd content toward the bulk. The reductive treatment induced a shift to higher BE even when comparing the as-prepared and the reduced states at the same photon energy, indicating the progress of surface and subsurface reconstruction due to the reduction of ZnO by H_2 and subsequent diffusion of Zn toward the bulk. The $Pd3d_{5/2}$ signals of the Zn-rich sample $Zn_{51.6}Pd_{48.4}$ were observed at the highest binding energies (336.6 eV at a photon energy of 1162 eV), while the $Pd3d_{5/2}$ signal of the Pd-rich sample $Zn_{49.8}Pd_{50.2}$ only reached 336.2 eV at the same photon energy. It is worthwhile to mention that the $Pd3d_{5/2}$ signal of $Zn_{49.8}Pd_{50.2}$ does not shift with increasing photon energy to the same extent as the Zn-richer samples. It can be assumed that the bulk-predetermined intermetallic state is reached, leading to a BE for $Pd3d_{5/2}$ of 336.2 eV. The atomic Zn/Pd ratios depending on the photon energy after reduction in hydrogen at 420 °C are shown in Fig. 5. The Zn-richest bulk sample possesses also the Zn-richest surface. For all samples, the near-surface content of Pd has increased during reduction compared to the "as-prepared" state (Fig. 2c), approaching the Pd-bulk content of the samples at the highest kinetic energy. Summarizing the *in situ* reduction of the $Zn_{100-x}Pd_x$ samples, it can be stated that the ability to completely reduce oxidized Zn on the surface is given for the Pd-richer samples, while the Zn-richer samples are strongly enriched in Zn on the surface, leading to formation of ZnO which cannot be reduced completely under the applied conditions.

3.3. Catalytic properties

Methanol steam reforming was carried out at atmospheric pressure in a flow reactor on unsupported, single-phase $Zn_{100-x}Pd_x$ samples. Catalytic experiments on as-prepared powders without any pretreatment showed poor activity in methanol steam reforming for most samples, which is not surprising if zinc oxide covers the surface. According to the XPS investigations, a reductive pretreatment in hydrogen is capable of reducing the ZnO content to reach a defined and reproducible surface state. All $Zn_{100-x}Pd_x$ samples were heated in flowing hydrogen (3 mL/min) up to 200 °C for 1 h. After a thorough purging with nitrogen, methanol steam reforming conditions were applied to the catalysts at 200 °C. Temperatures were increased to 500 °C with 2 K/min, while the product gas composition was monitored. Fig. 6 summarizes the catalytic activities of all investigated $Zn_{100-x}Pd_x$ samples as a function of the reaction temperature. Below 300 °C, activities were very low. The activity of $Zn_{40.9}Pd_{59.1}$ at 500 °C is 3 mmol H_2 per gram catalyst and hour, which corresponds to around 1% conversion of the $MeOH/H_2O$ feed, while the activity of $Zn_{53.2}Pd_{46.8}$ at the same temperature is close to 200 mmol H_2 $g^{-1}h^{-1}$, which corresponds to a $MeOH/H_2O$ conversion of 65%. The reason for the low activities of all $Zn_{100-x}Pd_x$ samples lies in the rather large particles of around 10 μm. When comparing the activities between 450 and 500 °C, the values were higher the higher the Zn content was in the intermetallic compounds. A major jump in activity by a factor of close to 10 is observed when the Pd content was lower than 49 at%. This significant difference can be explained by the existence of still oxidized Zn atoms on the surface of the Zn-rich samples, which allow easier adsorption of reactant molecules than on pure metallic surfaces facilitating the initial dissociation of MeOH and H_2O [29]. XPS results support this assumption because the Zn-richest of the $Zn_{100-x}Pd_x$ samples were not completely reduced even at temperatures of 420 °C, while reduction of the oxidized Zn atoms in the Pd-rich samples was found to be complete. When looking at the course of the activities in Fig. 6, two catalysts show unexpected low-temperature activity peaks

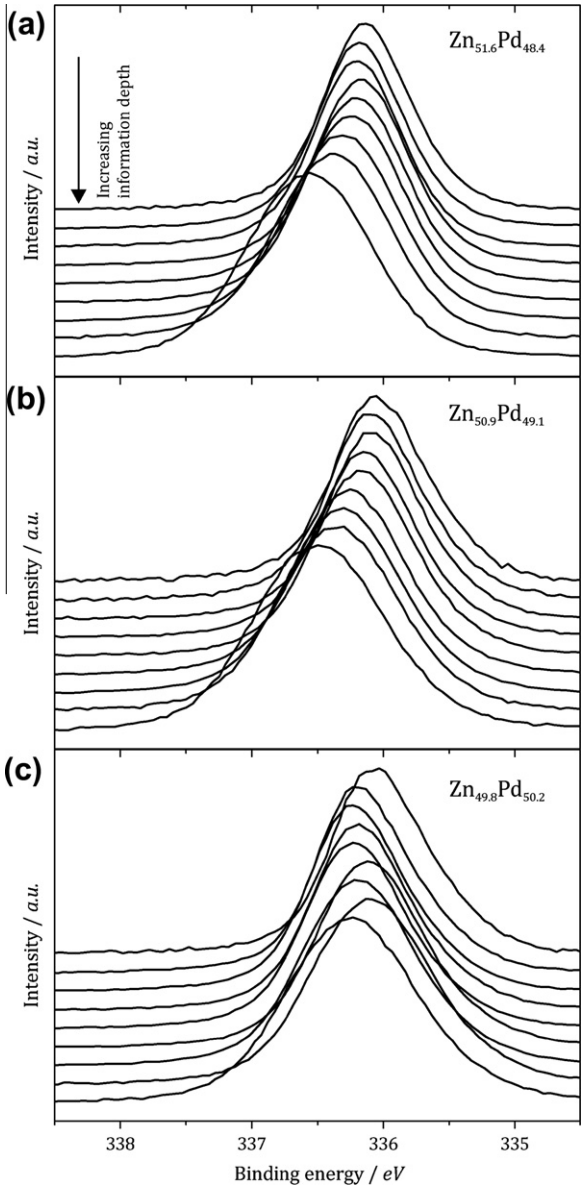

Fig. 4. Pd3d$_{5/2}$ region (depth profile by XPS) of: (a) $Zn_{51.6}Pd_{48.4}$, (b) $Zn_{50.9}Pd_{49.1}$ and (c) $Zn_{49.8}Pd_{50.2}$ after *in situ* reduction in H_2 (420 °C, 0.5 mbar). Top spectra are each recorded at 562 eV. Following spectra were recorded by increasing the photon energy stepwise by 75 eV.

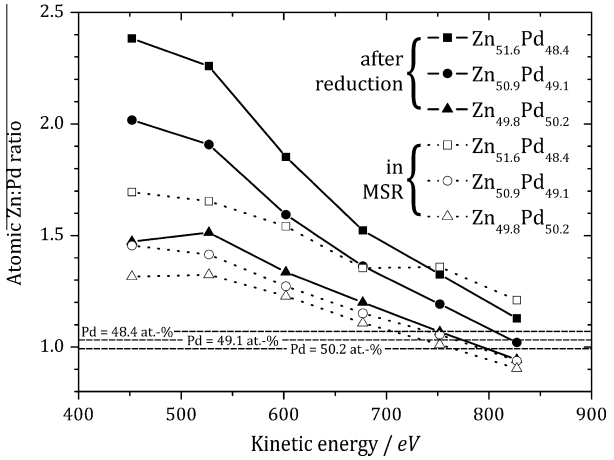

Fig. 5. Depth-depending atomic Zn/Pd ratio of $Zn_{51.6}Pd_{48.4}$, $Zn_{50.9}Pd_{49.1}$ and $Zn_{49.8}Pd_{50.2}$ after hydrogen reduction (420 °C, 0.5 mbar) and during methanol steam reforming (360 °C, 0.2 mbar, H_2O:MeOH = 2:1) derived from XPS measurements. Horizontal dashed lines represent the Pd bulk content of the investigated samples.

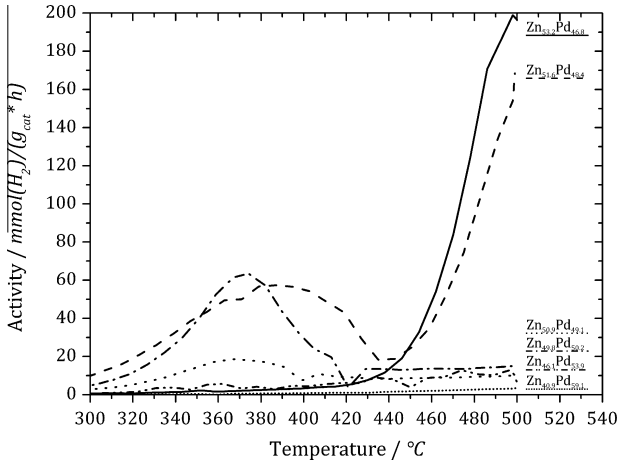

Fig. 6. Catalytic activity of $Zn_{100-x}Pd_x$ samples in methanol steam reforming (atmospheric pressure, H_2O:MeOH = 1:1).

below 400 °C. For $Zn_{49.8}Pd_{50.2}$, the activity at 370 °C was even higher than its activities at higher temperatures. The existence of two activity maxima in a temperature region is contradictive to classic catalyst behavior that usually follows a volcano plot. We suppose that optimized interactions between metallic and oxidized surface atoms are causing the high low-temperature activity. Naturally, these states can only be stable within a narrow parameter space. Increasing the temperature induced a self-reduction of the catalyst by the produced H_2. As a consequence, majorities of the oxidized Zn atoms were reduced and the activity dropped. The existence of dynamic surface states is supported by the hysteresis behavior as temperature profiles from 500 to 300 °C did not result in activity peaks below 400 °C (Fig. S3). Even an additional temperature cycle (200 °C → 500 °C → 200 °C) could not restore the low-temperature/high-activity features. This can be taken as indication that the catalysts are reduced in the course of the temperature-dependent activity measurement and finally expose an equilibrium surface state that possessed a certain amount of oxidized Zn atoms, according to the composition of the bulk intermetallic compounds. Metal/carbon ratios on the surface of the samples in UHV were in the regime of 1:4–1:8 – which is mostly due to a permanent carbon contamination in the *in situ* XPS cell – but did not change under MSR conditions, excluding a significant influence of carbon on the observed activity trends. The dependence of the catalytic properties on the composition of the samples becomes even more drastic when looking at the CO_2 selectivity of the $Zn_{100-x}Pd_x$ samples shown in Fig. 7. Since most of the samples showed only little activity at lower temperatures, an accurate selectivity determination becomes reasonable from 400 °C and above. Samples with higher Pd content (but without elemental Pd) showed decreasing CO_2 selectivity down to 10%, making them almost inactive for methanol steam reforming but active for methanol decomposition. This disagrees with all reports on ZnPd/ZnO, which do report high CO_2 selectivity as soon as the intermetallic compound is observed. As result, the presence of the intermetallic compound ZnPd alone is not sufficient for high selectivity in MSR, and the role of oxidized Zn species in the supported catalytic system will be further elucidated in a forthcoming publication. The highest CO_2 selectivity of 99.4%, corresponding to 1600 ppm CO in the product gas, was achieved on $Zn_{48.4}Pd_{51.6}$ between 350 and 400 °C in the low-temperature/high-activity region. The reason for the high selectivity (and activity) originates from the

optimized interaction on the interfaces between the electronically modified Pd atoms and oxidized Zn atoms. If zinc oxide on these Zn-rich samples is reduced by the H_2 which is formed during MSR, the CO_2 selectivity still reaches 98%. Despite being also rich in Zn on the surface, the surface Zn content is comparably lowered on the samples that are rich in bulk Pd leading to Pd arrangements that favor methanol decomposition rather than methanol steam reforming. This makes the absence of oxidized Zn on the surfaces of the Pd-rich samples likely to be the reason for the very low activities.

The catalysis data reveal that the small differences in bulk composition not only account for different electronic surface states and surface compositions as seen in XPS but also strongly affect the catalytic activity and selectivity at atmospheric pressure.

3.4. Surface analysis of reduced $Zn_{100-x}Pd_x$ under MSR conditions

Because of the often stated pressure gap, the assignment of catalytic properties that were determined at atmospheric pressure to surface states that were investigated at pressures of 10^{-8} mbar can only be reasonable, if the catalysts also show catalytic activity under reduced pressure conditions. Therefore, after the reduction procedure in the XPS cell, *in situ* experiments were continued under methanol steam reforming conditions at 0.2 mbar. For the investigated $Zn_{100-x}Pd_x$ samples, the surfaces were exposed to a $MeOH/H_2O$ mixture, and it was verified that the feed was at least partially converted to hydrogen and the corresponding carbon-containing products. One of the most important results was that the Zn3d signals for all samples remained almost unaffected under methanol steam reforming conditions. That is the preservation of oxidized Zn for the Zn-rich composition $Zn_{51.6}Pd_{48.4}$ still accounting for almost 10 at% of total Zn at the photon energy of 237 eV (Fig. S4). The Pd-richer samples revealed no change in spectra compared spectra recorded after reduction in hydrogen at 420 °C showing only intermetallic Zn. Considering the Zn/Pd surface ratio, it can be seen that the applied MSR conditions caused a Pd enrichment of the surface layers in all $Zn_{100-x}Pd_x$ samples when compared to the Zn/Pd ratio after hydrogen reduction (Fig. 5). Still, the trends for Zn-rich and Pd-rich samples remained. Comparison of the valence bands of all investigated samples under MSR conditions at the most surface-sensitive photon energy shows that the d-band of the Pd4d core-level is shifted away from the Fermi energy with decreasing Pd bulk content (Fig. 8). This shift is explained by the increasing number of valence electrons due to the increasing Zn content and leads to a lower density of states near the Fermi energy. Combining this observation with the catalytic results reveals a strong electronic influence on the activity as well as the selectivity of the compounds, i.e., the catalytic properties are drastically improved the further the valence band is shifted from the Fermi energy.

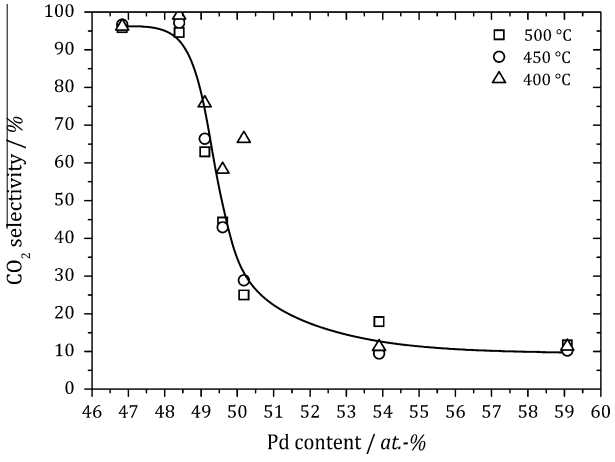

Fig. 7. CO_2 selectivity of $Zn_{100-x}Pd_x$ samples in methanol steam reforming depending on the reaction temperature (atmospheric pressure, H_2O:MeOH = 1:1). The line is a guide to the eye.

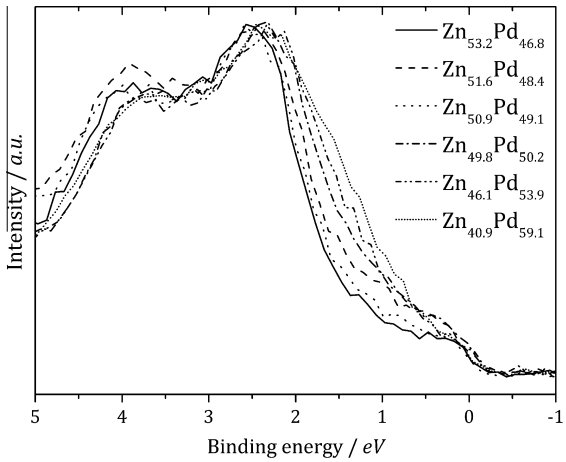

Fig. 8. XPS valence band region (photon energy = 237 eV) of $Zn_{100-x}Pd_x$ samples with different compositions under MSR conditions (0.2 mbar, H_2O:MeOH = 2:1).

4. Conclusions

Single-phase samples of the intermetallic compound ZnPd were prepared with different bulk compositions (47–59 at% Pd). XPS investigations were performed on as-prepared and reduced samples as well as under methanol steam reforming conditions, showing significant differences in Zn/Pd surface ratios, Pd3d binding energies and the amount of oxidized Zn species on the surface, depending on the bulk Pd content. All $Zn_{100-x}Pd_x$ (x = 46.8–59.1) samples preserved their intermetallic character in the near-surface region under MSR conditions. Compounds that are Zn-rich in bulk possess the Zn-richest surfaces and show the strongest shift in Pd3d binding energies compared to elemental Pd. Oxidized Zn species after reduction could only be observed on Zn-rich samples. These findings strongly correlate with the methanol steam reforming properties under atmospheric pressure: Samples rich in Zn showed highest activities and extraordinary high selectivity to CO_2, whereas samples rich in Pd only possessed poor catalytic activity and mainly formed CO during the reaction. A well -balanced equilibrium between oxidized Zn species and intermetallic Pd on the surface of a Zn-rich sample even resulted in CO_2 selectivity of 99.4%. The results clearly show that two factors are governing the catalytic properties of the intermetallic compound ZnPd: (1) the Zn/Pd ratio governs the electronic properties at the Fermi energy and is crucial for the selectivity in methanol steam reforming. (2) The interaction between the intermetallic compound and oxidized Zn on the surface is necessary to obtain highly active catalysts.

Acknowledgments

We acknowledge the Helmholtz Zentrum Berlin für Materialien und Energie – Electron storage ring BESSY II – for providing beamtime at the ISISS beamline (Project Nos. 2010_2_100164 and 2011_1_101013). Networking within the COST Action CM0904 "Network for Intermetallic Compounds as Catalysts in the Steam Reforming of Methanol" nurtured this publication. The authors thank Y. Grin and R. Schlögl for valuable suggestions.

Appendix A. Supplementary material

Supplementary data associated with this article can be found, in the online version, at doi:10.1016/j.jcat.2011.09.013.

References

[1] P. Gruss, Die Zukunft der Energie: Die Antwort der Wissenschaft. Ein Report der Max-Planck-Gesellschaft, C.H. Beck, München, 2008.
[2] H.-F. Oetjen, V.M. Schmidt, U. Stimming, F. Trila, J. Electrochem. Soc. 143 (1996) 3838–3842.
[3] J.-P. Shen, C. Song, Catal. Today 77 (2002) 89–98.
[4] H. Purnama, T. Ressler, R.E. Jentoft, H. Soerijanto, R. Schlögl, R. Schomäcker, Appl. Catal. A: Gen. 259 (2004) 83–94.
[5] N. Takezawa, N. Iwasa, Catal. Today 36 (1997) 45–56.
[6] N. Iwasa, N. Takezawa, Top. Catal. 22 (2003) 215–224.
[7] N. Iwasa, S. Masuda, N. Takezawa, React. Kinet. Catal. Lett. 55 (1995) 349–353.
[8] M. Behrens, M. Armbrüster, Methanol Steam Reforming, Catalysis for Alternative Energy Generation, Springer, 2011.
[9] K. Föttinger, J.A. van Bokhoven, M. Nachtegaal, G. Rupprechter, J. Phys. Chem. Lett. 2 (2011) 428–433.
[10] A.M. Karim, T. Conant, A.K. Datye, Phys. Chem. Chem. Phys. 10 (2008) 5584.
[11] T. Conant, A.M. Karim, V. Lebarbier, Y. Wang, F. Girgsdies, R. Schlögl, A. Datye, J. Catal. 257 (2008) 64–70.
[12] Y. Suwa, S. Ito, S. Kameoka, K. Tomishige, K. Kunimori, Appl. Catal. A: Gen. 267 (2004) 9–16.
[13] A.P. Tsai, S. Kameoka, Y. Ishii, J. Phys. Soc. Jpn. 73 (2004) 3270–3273.
[14] S. Kameoka, T. Kimura, A.P. Tsai, Catal. Lett. 131 (2009) 219–224.
[15] B. Halevi, E.J. Peterson, A. DeLaRiva, E. Jeroro, V.M. Lebarbier, Y. Wang, J.M. Vohs, B. Kiefer, E. Kunkes, M. Hävecker, M. Behrens, R. Schlögl, A.K. Datye, J. Phys. Chem. C 114 (2010) 17181–17190.
[16] E.J. Peterson, B. Halevi, B. Kiefer, M.N. Spilde, A.K. Datye, J. Peterson, L. Daemen, A. Llobet, H. Nakotte, J. Alloys Compd. 509 (2011) 1463–1470.
[17] C. Rameshan, W. Stadlmayr, C. Weilach, S. Penner, H. Lorenz, M. Hävecker, R. Blume, T. Rocha, D. Teschner, A. Knop-Gericke, R. Schlögl, N. Memmel, D. Zemlyanov, G. Rupprechter, B. Klötzer, Angew. Chem. Int. Ed. 49 (2010) 3224–3227.
[18] W. Stadlmayr, C. Rameshan, C. Weilach, H. Lorenz, M. Hävecker, R. Blume, T. Rocha, D. Teschner, A. Knop-Gericke, D. Zemlyanov, S. Penner, R. Schlögl, G. Rupprechter, B. Klötzer, N. Memmel, J. Phys. Chem. C 114 (2010) 10850–10856.
[19] M. Armbrüster, K. Kovnir, M. Behrens, D. Teschner, Y. Grin, R. Schlögl, J. Am. Chem. Soc. 132 (2010) 14745–14747.
[20] K. Kovnir, M. Armbrüster, D. Teschner, T.V. Venkov, L. Szentmiklósi, F.C. Jentoft, A. Knop-Gericke, Y. Grin, R. Schlögl, Surf. Sci. 603 (2009) 1784–1792.
[21] M. Friedrich, A. Ormeci, Y. Grin, M. Armbrüster, Z. Anorg. Allg. Chem. 636 (2010) 1735–1739.
[22] L.G. Akselrud, Yu.P. Zavalii, Y.N. Grin, V.K. Pecharski, B. Baumgartner, E. Wölfel, Mater. Sci. Forum 133–136 (1993) 335–342.
[23] M. Salmeron, R. Schlögl, Surf. Sci. Rep. 63 (2008) 169–199.
[24] Casa XPS Version 2.3.16, 2010.
[25] J.J. Yeh, I. Lindau, Atom. Data Nucl. 32 (1985) 1–155.
[26] D. Teschner, E. Vass, M. Hävecker, S. Zafeiratos, P. Schnörch, H. Sauer, A. Knop-Gericke, R. Schlögl, M. Chamam, A. Wootsch, A.S. Canning, J.J. Gamman, S.D. Jackson, J. McGregor, L.F. Gladden, J. Catal. 242 (2006) 26–37.
[27] H. Gabasch, W. Unterberger, K. Hayek, B. Klötzer, E. Kleimenov, D. Teschner, S. Zafeiratos, M. Hävecker, A. Knop-Gericke, R. Schlögl, J. Han, F.H. Ribeiro, B. Aszalos-Kiss, T. Curtin, D. Zemlyanov, Surf. Sci. 600 (2006) 2980–2989.
[28] E. Galloway, M. Armbrüster, K. Kovnir, M.S. Tikhov, R.M. Lambert, J. Catal. 261 (2009) 60–65.
[29] G.K. Smith, S. Lin, W. Lai, A. Datye, D. Xie, H. Guo, Surf. Sci. 605 (2011) 750–759.